Available online at www.sciencedirect.com
SCIENCE DIRECT
Polymer 46 (2005) 9144–9154
polymer
www.elsevier.com/locate/polymer

The role of the hydrogen bonding network for the shear modulus of PIPD

J.C.L. Hageman[a], G.A. de Wijs[a,*], R.A. de Groot[a,b], E.A. Klop[c]

[a]*Institute for Molecules and Materials, Faculty of Science, Radboud University Nijmegen, Toernooiveld 1, 6525 ED Nijmegen, The Netherlands*
[b]*Laboratory of Chemical Physics, Materials Science Center, Nijenborgh 4, 9747 AG Groningen, The Netherlands*
[c]*Teijin Twaron BV, Fiber Physics Group, Dept. QRS, P.O. Box 9600, 6800 TC Arnhem, The Netherlands*

Received 22 March 2005; received in revised form 8 July 2005; accepted 9 July 2005
Available online 10 August 2005

Abstract

Ab initio total energy calculations at the DFT-GGA level for PIPD are reported. Both the monoclinic crystal with a bi-directional hydrogen-bond network and the triclinic crystal with a sheet-like network are studied. It is concluded that the latter is the more plausible microstructure for the fibre based on the following: (i) After optimisation of the lattice parameters and atomic positions it has a lower energy. (ii) The calculated internal shear modulus agrees better with experiment. (iii) The minimal shear stiffness constant, which is interpreted as the upper limit on the compressive strength, compares favourably with the experimental compressive strength.

The hydrogen bonding network plays a crucial—but indirect—role in explaining the high compressive strength. It replaces the weak components of the lateral bonding, such as present in many high performance polymer materials with low compressive strength, e.g. PBO and PBZT, with much stronger hydrogen bonds. This makes that in PIPD the relatively strong π–π interaction has the weakest resistance against shear.
© 2005 Elsevier Ltd. All rights reserved.

Keywords: PIPD; Mechanical properties; Hydrogen bonding network

1. Introduction

High performance polymer fibres form an important class of materials with excellent mechanical properties. The new member of this family, the recently developed [1] rigid-rod polymer poly(pyridobisimidazole) (PIPD), shows excellent tensile and compressive properties [2]. The tensile properties of PIPD, modulus of approximately 300 GPa and strength of 4.5 GPa, are comparable with that of its predecessors PBO and PBZT. The chemical structure of PIPD is shown in Fig. 1.

The essential difference between PIPD and its predecessors is the intermolecular hydrogen bonding network. This network is believed to lead to a higher torsion modulus and to improved compressive properties. Indeed, the compressive strength of PIPD is 1.7 GPa [2], whereas that of its predecessors is about 0.2–0.4 GPa [3].

Using diffraction studies, the topology of the hydrogen bonding network was studied by Klop et al. [4], and recently by Takahashi [5,6]. Based on analysis of their experimental data, Klop et al. concluded that their X-ray diffraction (XDR) patterns allowed for two different hydrogen bonding networks, hence two possible polymer crystal structures: A monoclinic crystal containing a bi-directional hydrogen bonding network and a triclinic crystal, wherein the hydrogen bonding network forms a sheet-like structure. Both structures are schematically depicted in Fig. 2. Based on the temperature dependence of the XRD patterns Klop et al. concluded that the bi-directional hydrogen bonding network was the most plausible.

In his X-ray diffraction study Takahashi [6] concluded that the intramolecular hydrogen bonds in PIPD are formed between NH and O, instead of between N and OH, as reported by Klop et al. [4] According to Takahashi the hydroxyl groups are rotated by (approximately) 180° compared to the conformation reported in Ref. [4]. Clearly the different hydroxyl group conformation would not only affect the intramolecular hydrogen bonds, but it would also alter the intermolecular hydrogen bonds. In Takahashi's

* Corresponding author. Tel.: +31 24 36 52984; fax: +31 24 36 52120.
E-mail address: g.dewijs@science.ru.nl (G.A. de Wijs).

0032-3861/$ - see front matter © 2005 Elsevier Ltd. All rights reserved.
doi:10.1016/j.polymer.2005.07.027

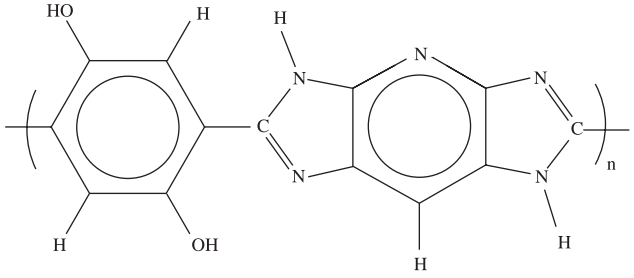

Fig. 1. The chemical structure of PIPD. The two OH groups of the dihydroxyphenylene moiety (left) and the two H atoms connected to nitrogens in the diimidazopyridinylene moiety (right) can participate in inter-molecular hydrogen bonds.

study the conformation of the hydroxyl groups was derived from neutron diffraction data reported in an earlier study by the same author [5]. In the latter paper the determination of the conformation of the hydroxyl groups was based solely on equatorial neutron diffraction data, and not on the full 2D neutron diffraction pattern. The parameter-data ratio was unfavourable and the standard deviation in the internal rotation angles of the hydroxyl groups ranged from 85 to 196°. In view of these large standard deviations the hydroxyl group conformation and the associated hydrogen bonding scheme as proposed by Takahashi [5,6] is questionable. Moreover, there is strong XRD and spectroscopic evidence that hydroxyl groups in the hydroxyphenylbenzothiazolyl unit (which is similar to the hydroxyphenylpyridobisimidazole unit in PIPD) form intramolecular hydrogen bonds between N and OH [7].

Takahashi's model of the PIPD crystal structure not only differs in the conformation of the hydroxyl groups since he also proposes a different disorder model. Positional disorder in PIPD was already proposed by Klop et al., as these authors reported that the pyridine *N* and –CH may be interchanged going from one repeat unit to the next [Ref. [4], p. 5991]. However, this type of disorder does not alter the hydrogen bonding scheme, since the pyridine N cannot act as hydrogen bond acceptor due to the axial shifting of the polymer molecules. The two crystal structures proposed by Klop et al. are supported by ab initio calculations [8]. These calculations indicate that both the monoclinic crystal and the triclinic crystal may co-exist in the fibre since their energy difference turned out to be very small. In the present paper we address the question whether the two different structures would lead to different torsion moduli and compressive strengths. And if so, what structure would explain the experimental properties of the fibre, that is a torsion modulus of 7.4 GPa and a compressive strength of 1.7 GPa [2]. Answers to these questions might elucidate what structural model would be appropriate to describe the PIPD fibres and why the hydrogen bonding network is crucial.

The determination of the torsion modulus and compressive strength from ab initio total energy calculations is performed in three steps. First, equilibrium structures are found by optimisation of both lattice parameters and atomic positions[1]. Then, several stiffness constants for the crystal structures are determined by applying small deformations to the equilibrium structures. Finally, these elastic constants are used to determine the internal shear modulus of perfectly oriented fibres containing these crystals, as well as the compressive strength using the model of DeTeresa et al. [9].

2. Computational details

The results presented in this paper were obtained with the ab initio total energy and molecular dynamics program VASP (Vienna ab initio simulation package) [10–13].

The behaviour of the electrons is described with density functional theory (DFT). The generalised gradient approximation (GGA) of Perdew and Wang [14] (PW) is used in order to treat the hydrogen bonds appropriately.

The atomic cores are described with ultrasoft Vanderbilt pseudopotentials [15,16]. A plane wave basis set including waves with a kinetic energy up to 38 Ry is used. The crystal structure is described by applying periodic boundary conditions on the unit cell. The Brillouin zone integrals are calculated as a summation over 8 *k*-points.

The volume of the unit cell is fixed to the XRD value [4] of 499 $Å^3$ during optimisation, since it is known that DFT-GGA would overestimate the volume due to lack of attractive dispersive forces [17]. An attempt of relaxing the volume demonstrated that the problem occurs here also. The volume turned out to be more than 20% larger than the experimental volume.

The stiffness constants are calculated from the total energy change upon imposing small, volume conserving deformations. Only those deformations that give rise to a negligible contribution of the dispersive interactions to the total energy change will yield reliable stiffness constants. The only stiffness constants considered are for shearing along the *z*-axis, i.e. the molecular chain axis. For the deformations pertaining to these shears, the dominant interchain interactions are the hydrogen bonds and the interactions between the π-systems. The dispersive (van der Waals) interactions can be neglected.

3. Crystal structure optimisation

From XRD studies [4] the monoclinic structure with the bi-directional hydrogen bonding network seems to be the more plausible. Previous ab initio calculations [8] indicated that of the two experimental structures the triclinic structure would be energetically favourable (about 5 meV for the Perdew–Wang GGA), however, we did not allow for

[1] In a previous paper [8] the atomic positions were optimised at fixed lattice parameters.

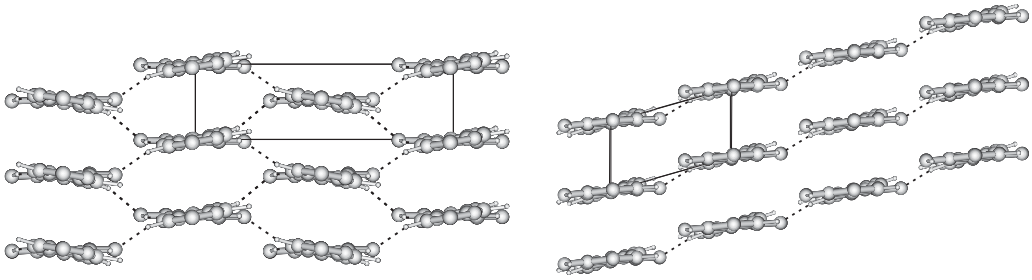

Fig. 2. Monoclinic (left) and triclinic (right) structures, viewed along the molecular axis. Hydrogen bonds are indicated as dashed lines.

changes in the crystal structure—i.e. we fixed the lattice parameters. In this work we allow the lattice parameters to change during optimisation at fixed volume.

As starting point we chose the experimentally more plausible monoclinic unit cell containing two monomers. The XRD determined lattice parameters were used ($a=12.60$ Å, $b=3.48$ Å, $c=12.01$ Å, $\alpha=90°$, $\beta=108.6°$ and $\gamma=90°$). All atomic positions were relaxed and the energy of this unit cell is taken as reference, i.e. zero point of energy. This crystal is referred to as the XRD crystal.

Next, both the unit cell as well as the atomic positions were optimised under the constraint that the monoclinic symmetry was conserved. This led to a unit cell with the parameters $a=11.80$ Å, $b=3.63$ Å, $c=12.07$ Å, $\alpha=90°$, $\beta=105.3°$ and $\gamma=90°$. The resulting hydrogen bonding network was bi-directional like in the XRD crystal. The resulting energy was -219 meV.

A second optimisation was started from an experimental unit cell that was deformed in such a way that the angle α was no longer 90°. After optimisation the lattice parameters were $a=11.75$ Å, $b=3.79$ Å, $c=12.09$ Å, $\alpha=105.0°$, $\beta=103.4°$ and $\gamma=77.2°$. During this optimisation the bi-directional hydrogen bonding network transformed to the sheet-like form in the triclinic unit cell as was proposed by Klop et al. [4] and was found previously [8]. The energy of this structure is -431 meV.

The energy difference between the monoclinic and triclinic structure is 212 meV, where the triclinic is the lowest in energy. This is in qualitative agreement with our previous results [8], but the difference is larger due to the lattice relaxation.

Why the triclinic crystal is more stable than the monoclinic crystal cannot be understood from a simple model. Many interactions are in competition: The chains prefer to be flat, where the bi-directional hydrogen network causes a torque leading to torsion. The π-systems prefer to be not exactly on top of each other (as we will see in Section 6), which can be solved by either a shift of the chains (triclinic crystal) or perhaps a rotation of the π-systems (monoclinic crystal). And also steric hindrance might play a role.

In Fig. 3 the XRD patterns resulting from the crystal structures described above are compared with the experimental pattern. The XRD patterns are calculated with the Cerius2 software (version 4.2) from Molecular Simulations as done previously by Klop et al. [4]. As expected, the calculated pattern of the XRD crystal has the best overall agreement with the experimental pattern. However, the wide-angle meridian reflections are better described by the triclinic structure than by the two monoclinic crystals. This is due to the fact that the angle α is not restricted to be 90°. On the other hand the two monoclinic structures describe the off meridian reflections at small angles better. This is a result of the fact that the *ab* projection of the unit cell is better described in the monoclinic crystals. On basis of the XRD patterns of Fig. 3 it is not possible to discriminate between the two ab initio calculated structures.

In summary, an energy difference between the two ab initio determined crystals exists and is substantial (45 K/atom on a temperature scale). Based on this result it is more likely that the triclinic crystal will be found in the fibres. Comparison of the XRD patterns does not show a clear preference. Since temperature dependent XRD measurements suggested that the monoclinic crystal is in favour, both structures are considered possibly relevant in the following part.

4. Shear stiffness of the crystals

The elastic tensor is defined as the relationship between the stress tensor σ_κ and the strain tensor ε_λ for small strains [18]:

$$\sigma_\kappa = \sum_{\kappa,\lambda} C_{\kappa\lambda}\varepsilon_\lambda \tag{1}$$

where the Voigt notation $C_{\kappa\lambda}$ is adopted, the labels run from 1 to 6.[2]

In the harmonic approximation the energy of a unit cell can be written as

$$E(\varepsilon) = \frac{1}{2}V\sum_{\kappa,\lambda} C_{\kappa\lambda}\varepsilon_\kappa\varepsilon_\lambda \tag{2}$$

where V is the volume of the unit cell at equilibrium and the energy of the unit cell at equilibrium is taken to be zero. This energy expression can be used to calculate the elastic

[2] It should be noted that $C_{\kappa\lambda}$ is not a tensor and cannot be used in a tensor transformation. In order to perform a transformation the elastic matrix $C_{\kappa\lambda}$ has to be rewritten as a tensor of the rank 4.

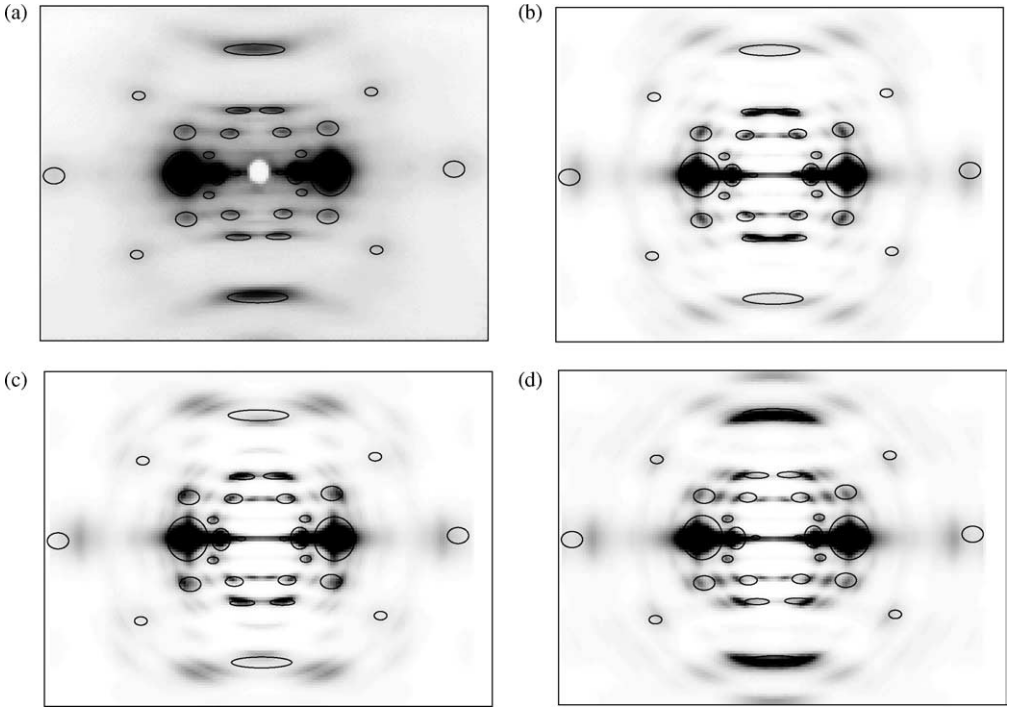

Fig. 3. Comparison of the XRD patterns for the different crystal structures: (a) The experimental XRD pattern, (b) the calculated pattern for the proposed monoclinic crystal by Klop et al. [4] (the XRD crystal), (c) the ab initio optimised monoclinic crystal and (d) the ab initio optimised triclinic crystal. The crystallite size, orientation and temperature are chosen to match the experimental pattern. As a visual aid a caricature of the experimental pattern is given by the solid lines.

constants by applying small specific strains to the equilibrium structure and calculating the total energy change.

A strain ε is applied to the crystal by deforming the primitive vectors ($\mathbf{a}_k$) according to

$$\mathbf{a}'_k = (1 + [\varepsilon])\mathbf{a}_k \tag{3}$$

where $[\varepsilon]$ is the strain tensor in matrix notation [18]:

$$\begin{bmatrix} \varepsilon_1 & \frac{1}{2}\varepsilon_6 & \frac{1}{2}\varepsilon_5 \\ \frac{1}{2}\varepsilon_6 & \varepsilon_2 & \frac{1}{2}\varepsilon_4 \\ \frac{1}{2}\varepsilon_5 & \frac{1}{2}\varepsilon_4 & \varepsilon_3 \end{bmatrix} \tag{4}$$

In particular, if the strain $\varepsilon_\lambda = \delta$ is applied—and all others are zero—the energy expression takes a simple form:

$$E = \frac{1}{2} V C_{\lambda\lambda} \delta^2 \tag{5}$$

We calculate the total energy as a function of strain for several values of δ. For each δ the cell dimensions are fixed but all atomic positions are relaxed. From a least-squares fit of a quadratic function to the resulting data points the elastic constant $C_{\lambda\lambda}$ is obtained. All data points were taken to have a weight one. The standard deviation is taken as the measure for the uncertainty in the fit parameter.

This technique is often applied for simple inorganic compounds, where the elastic constants are usually considerably larger and typical values of δ are very small ($\delta < 0.01$). In the present calculation, however, the energy differences are very small (the energies in Figs. 4–6 pertain to a 54 atoms cell) and we needed to allow larger displacements to reduce numerical noise. We took care to remain in the harmonic régime and checked with both positive and negative displacements and allowed for a total of seven data points.

For the monoclinic crystal the energy as function of ε_4

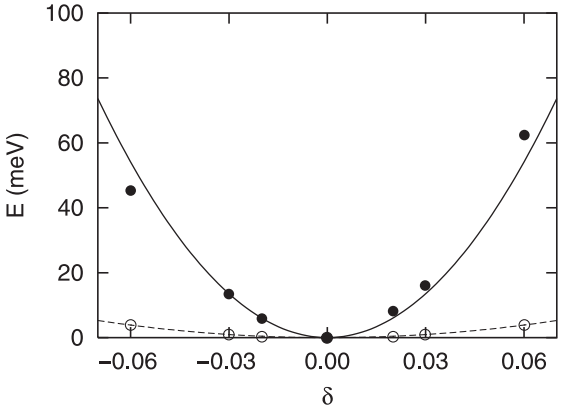

Fig. 4. The energy per unit cell of the monoclinic crystal as function of the size of the strain. The open circles are the data for ε_4 and the full circles for ε_5. The lines are the least-square fits of a quadratic function for ε_4 (dashed line) and ε_5 (solid line).

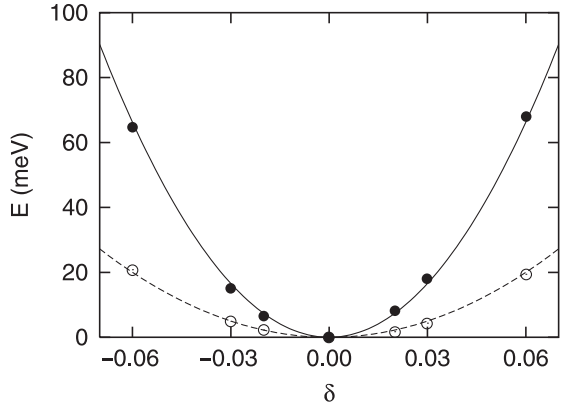

Fig. 5. The energy per unit cell of the triclinic crystal as function of the size of the strain. The open circles are the data for ε_4 and the full circles for ε_5. The lines are the least-square fits of a quadratic function for ε_4 (dashed line) and ε_5 (solid line).

and ε_5 is shown in Fig. 4. The anisotropy of the elasticity is clearly seen and the two elastic constants are $C_{44}=0.690\pm 0.006$ GPa and $C_{55}=9.65\pm0.62$ GPa. The crystal deviates significantly from Hookean elasticity in case of ε_5, leading to a relatively large uncertainty in the elastic constant. If a third order term is included in order to account for the anharmonicity, then the elastic constant is $C_{55}=9.65\pm 0.14$ GPa.

For the triclinic crystal the energy curves are shown in Fig. 5. The resulting elastic constants are $C_{44}=3.57\pm 0.06$ GPa and $C_{55}=11.82\pm0.17$ GPa. Again anisotropy can be observed. The deviations from Hookean elasticity are much smaller in this case.

Since only 8 k-points are used it is checked what the effect is upon doubling of the number of k-points per direction. The largest change in energy difference between configurations was smaller than 0.2 meV. An error in the energy of 0.2 meV at $\delta=0.02$ would lead to a change in the elastic constant of 0.32 GPa (from Eq. (5)). This is a measure of the accuracies that are obtained.

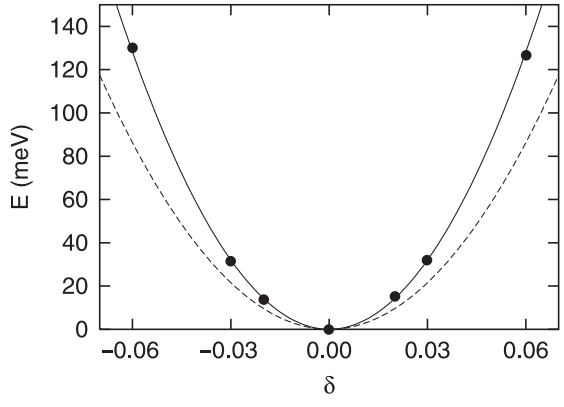

Fig. 6. The energy per unit cell of the triclinic crystal as function of the size of the strains ε_4 and ε_5 simultaneously. The full circles are the ab initio data. The solid line is the quadratic fit and the dashed line is the energy that stems from C_{44} and C_{55}.

In order to make a fair comparison between the elastic constants of the crystal it is important to realize that due to the anisotropy the shear stiffness constants depend on the orientation around the chain axis (which we place along the z-axis). This orientation can be characterised by an angle θ. The shear stiffness constants then take the form

$$C_{44}(\theta) = C_{44}(0)\cos^2\theta + C_{55}(0)\sin^2\theta + 2C_{45}(0)\cos\,\theta\,\sin\,\theta \tag{6}$$

$$C_{55}(\theta) = C_{55}(0)\cos^2\theta + C_{44}(0)\sin^2\theta - 2C_{45}(0)\cos\,\theta\,\sin\,\theta \tag{7}$$

and

$$C_{45}(\theta) = C_{45}(0)(\cos^2\theta-\sin^2\theta) + (C_{55} - C_{44})\cos\,\theta\,\sin\,\theta \tag{8}$$

To compare the two crystals fairly we should compare the maximum and minimum values for the shear stiffness constants:

$$C_{\pm} = \frac{C_{44}+C_{55}}{2} \pm \sqrt{\frac{(C_{44}-C_{55})^2}{4} + C_{45}^2} \tag{9}$$

Evaluation of Eq. (9) requires C_{45}. In order to calculate C_{45} the strains $\varepsilon_4=\delta$ and $\varepsilon_5=\delta$ are applied simultaneously. This leads to an energy expression:

$$E = \frac{1}{2}V(C_{44}+C_{55}+2C_{45})\delta^2 \tag{10}$$

Calculating the energy as function of δ then gives C_{45}.

For the monoclinic crystal C_{45} should be formally zero [18]. Using the above procedure leads to $C_{45}=-0.20\pm 0.29$ GPa, which is indeed zero within the limits of accuracy. This result is a validation of the procedure. The minimal stiffness constant is thus $C_-=C_{44}=0.69$ GPa, whereas the maximal is $C_+=C_{55}=9.65$ GPa.

For the triclinic crystal the energy dependence is plotted in Fig. 6. The elastic constant is calculated to be $C_{45}=3.74$ GPa. The minimum and maximum shear stiffness constants can be calculated, for the triclinic case, to be $C_-=2.13$ GPa and $C_+=13.26$ GPa. These values are significantly different from C_{44} and C_{55}.

Comparison of the stiffness constants for the triclinic structure and the monoclinic structure shows a significant difference. The triclinic structure has the larger constants, both minimal and maximal. The minimal stiffness constant of the triclinic structure is a factor three larger than that of the monoclinic structure. The maximal constants differ about 30%.

5. Fiber properties

In this section the calculated shear moduli of the triclinic crystal (sheet-like hydrogen bonding network) and the monoclinic crystal (bi-directional hydrogen bonding network) are compared with the experimental data on the PIPD fibre by Lammers et al. [2]. First, the results are compared with the experimental data on the shear modulus. Second, the results are used to estimate the compressive strength and this is compared with the experimental result.

5.1. Internal shear modulus

Lammers et al. [2] have determined the experimental value of the shear modulus and the elastic modulus of the crystallites in the following way: For fibres of different orientation they have measured the elastic modulus of the fibre (E) in a tensile test and, using XRD, have determined the second moment of the orientation of the filaments with respect to the fibre axis ($\langle \sin^2\phi \rangle$). The linear relation between the fibre modulus and the orientation is given by Ref. [19]:

$$\frac{1}{E} = \frac{1}{e_c} + \frac{\langle \sin^2\phi \rangle}{2g} \tag{11}$$

where e_c is the elastic modulus of the crystallites and g the internal shear modulus, for which it is assumed that the crystallites possess fibre symmetry, i.e. they are isotropic perpendicular to the fibre axis. Using this relationship the two moduli e_c and g are obtained.

Because fibre symmetry is assumed only one modulus (g) is sufficient to characterise the behaviour under shear. Moreover, g can be directly related to the stiffness (C) and the compliance (S) matrix:

$$g = C^f_{44} = C^f_{55} = \frac{1}{S^f_{44}} = \frac{1}{S^f_{55}} \tag{12}$$

Here the superscript f denotes fibre symmetry.

The monoclinic and triclinic crystals do not possess fibre symmetry. To allow for a comparison of the calculated shear stiffness with the measured shear modulus g, a fibre-symmetric crystallite is constructed by assuming that, in turn, it consists of many crystallites with the real crystal properties. It is assumed that: (a) All crystallites have their chain axis and the fibre axis coincide ($\phi = 0$) and (b) all orientations (θ) around the chain axis are equally present. For such a perfectly oriented crystallite with random lateral texture the internal shear modulus g equals the torsion modulus. It is appropriate to refer to g as the internal shear modulus as it is actually a property of the crystallite.

Averaging over all orientations θ of the crystallites gives the internal shear modulus

$$g = C^f_{44} = C^f_{55} = \frac{C_{44} + C_{55}}{2} \tag{13}$$

where C_{44} and C_{55} now pertain to the real crystal properties and

$$C^f_{45} = 0 \tag{14}$$

as it should be according to fibre symmetry.

Since the internal shear modulus as determined by Lammers et al. corresponds to the average of the shear moduli of the crystals, the calculated moduli can easily be compared with the experimental data. For a fibre consisting of crystallites with a bi-directional hydrogen bonding network, the monoclinic shear moduli predict an internal shear modulus g of 5.17 GPa. For a fibre consisting of crystallites with sheet-like hydrogen bonding networks, the triclinic shear moduli predict an internal shear modulus of 7.70 GPa.

The calculated shear moduli are both of the same order of magnitude as the experimental value of 7.4 ± 0.9 GPa. The triclinic structure agrees quantitatively with this experiment, whereas the modulus of the monoclinic structure is too low. This makes the triclinic structure more probable.

It should be noted that from ultrasonic velocity measurements [20] on a PIPD/epoxy composite the shear modulus of the fibre was calculated to be 5.2 ± 0.7 GPa, which coincides with the calculated value of the monoclinic structure. However, this is the shear modulus of a fibre with an elastic modulus C_{33} of 285 GPa and not of the crystallite, which has an elastic modulus C^c_{33} over 500 GPa [2].

5.2. Compressive strength

DeTeresa et al. [9] have argued that compressive failure of extended chain polymers is due to an elastic buckling instability, analogous to the Euler buckling of an elastic rod [21]. DeTeresa et al. modeled a polymer fibre as a collection of polymer chains forming a tetragonal lattice supported by an elastic foundation. The foundation was used to introduce the effect of interchain interaction. It was shown that the instability occurred when the stress exceeded the value of the relevant shear modulus, in their model the torsion modulus g.

Indeed, in experiment a linear relationship is found between the torsion modulus and the compressive strength. However, the torsion modulus overestimated the compressive strength with a factor of three for PPTA [9].

DeTeresa et al. have used a tetragonal lattice and thus the following relationship holds [18]:

$$g = C_{44} = C_{55} \tag{15}$$

Although this is also true in the case of fibre symmetry, this is not true for the crystals that constitute the fibre. Since the fibre fails when the constituting crystallites fail, it is the compressive strength of the crystals that determines the compressive strength of the fibre. This was realized by Lacks [22]. He showed with molecular mechanics simulations that for orthorhombic PPTA the instability occurs in

the direction with lowest shear modulus and that this modulus gives the threshold value for the elastic buckling instability. The calculated threshold [22] (0.34 GPa) agrees with the experimental compressive strength (0.3–0.4 GPa) [3].

In order to extract useful information from the calculated shear stiffnesses of PIPD from the model by DeTeresa et al. it needs to be generalised to arbitrarily low-symmetry (i.e. monoclinic and triclinic). Starting point is the energy change upon applying a general shear (Eq. (A34) in DeTeresa et al.) in which—at variance with DeTeresa et al.—we now assume a completely general deformation:

$$E = \frac{1}{2}\sum_{\lambda}\int_{V}\sigma_\lambda\varepsilon_\lambda \mathrm{d}V \tag{16}$$

Using Eq. (1) this gives:

$$E(\varepsilon) = \frac{1}{2}\sum_{\lambda,\kappa}\int_{V}C_{\kappa\lambda}\varepsilon_\kappa\varepsilon_\lambda \mathrm{d}V \tag{17}$$

which is the continuum generalisation of Eq. (2). Following Lacks, we search for a plane in which the resistance against buckling is minimal. The coordinate system is rotated until a minimal $C_{\lambda\lambda}$ is found. We then only consider the specific shear stress ε_λ and thus retrieve DeTeresa's model so that $C_{\lambda\lambda}$ gives the compressive strength. In doing so, cross terms $C_{\kappa\lambda}$, i.e. buckling patterns that cannot be confined to a plane, have been neglected and, therefore, an upper bound on the compressive strength is found. Moreover, as an additional simplification, only rotations around the chain axis are considered. Again, this means that an upper bound is obtained. However, for PIPD it is not likely that other rotations will provide possibilities for an easier shear deformation: Any shear in a plane tilted away from the molecular chain axis will incur a non-zero tensile load on the molecular chains themselves, and it is known—because of the high Young's modulus—that such deformations are energetically very unfavourable.

According to the above generalisation, the upper limits to the compressive strength are just the minimal shear stiffnesses C_{-} that were obtained in Section 4. For a sheet-like network structure this implies an upper limit on the compressive strength of 2.1 GPa and for the bi-directional network 0.7 GPa. The number for the sheet-like, triclinic structure compares favourably with the experimental value of 1.7 GPa, whereas the upper limit for the bi-directional network is much too low.

The main advantage of the model by DeTeresa et al. is that it provides a simple physical mechanism that allows for predictions on the strength of a polymer fibre directly from microscopic properties of the polymer crystal. It is based on several assumptions, as it models the geometric (buckling) instability of one polymer chain immersed in an essentially isotropic environment of neighbor chains. The geometric instability is of *elastic* origin. It is assumed that this instability, practically concurring with larger deformations, starts-off irreversible damage, leading to fibre failure. The orientation dependence of the shear interaction (i.e. non-isotropic surrounding) has been dealt with for the main part with the above generalisation inspired by Lacks. However, we still have to assume the neglect of edge-effects (polymer chains at the outside of the crystal experience a different shear) and assume perfect crystalline order within the crystallite, i.e. no defects (misalignments, etc). These may result in local stress accumulation and eventually in fibre failure. Another drawback of the model is that it disregards the disorientation as described by the orientation distribution of the crystallites (on which Eq. (11) is based). A combination of the fibre model of Northolt et al. [19,23,24] with the failure mechanism from DeTeresa's model is expected to provide a more realistic description of the yielding behaviour of PIPD fibres. As a final note we like to point out that all assumptions made and effects neglected consistently point to an underestimation of the true compressive strength, i.e. the model is expected to provide an upper limit on the compressive strength.

6. Interchain interactions

In order to get an impression of the interchain bonding in the crystal the present results are mapped onto a model containing nearest neighbour and next-nearest neighbour bonds. Fig. 7 shows a schematic picture of the crystals in the lateral direction as well as the force constants used in the model. The energy is assumed to depend on the shift of the chains with respect to each other and is written as

$$E = \frac{1}{2}K_1(\Delta s_1^2 + \Delta s_4^2) + \frac{1}{2}K_2(\Delta s_2^2 + \Delta s_5^2) + \frac{1}{2}K_3(\Delta s_3^2 + \Delta s_6^2) \tag{18}$$

where Δs_i is the shift out of equilibrium of chain i with

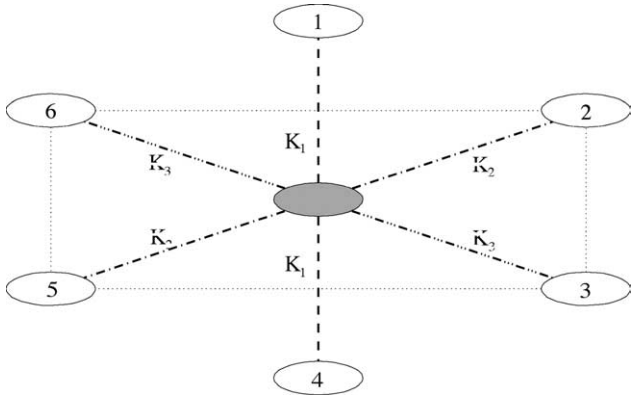

Fig. 7. Schematic representation of the next-nearest neighbour model. The lateral directions of the crystals is drawn and the different force constants between the chains are distinguished.

respect to the central chain at a given strain. Applying a shear strain to the crystal, the shifts of the chains are calculated. Then the force constants can be chosen to reproduce the ab initio calculated shear stiffness constants, using Eqs. (5) and (10). The calculated force constants depend little on the applied strain (1% for a change of 5% strain) and the limit for the strain to zero is taken.

For the bi-directional hydrogen bonding network the elastic constants are $C_{44}=0.69$ GPa, $C_{55}=9.65$ GPa and $C_{45}=0$ GPa. This leads to force constants $K_1=-0.035$ eV/Å^2 and $K_2=K_3=0.232$ eV/Å^2. The two diagonals are equivalent as required from symmetry. The fact that K_1 is negative supports the idea that the nearest neighbour chains (i.e. the chains differing a vector **b**) prefer to be shifted. The interchain bonding along the diagonals of the unit cell is large enough to ensure that the total energy rises upon increasing the strain ε_4. In other words the next-nearest neighbour bonding stabilises the crystal under shear.

For the sheet-like network (triclinic structure) the elastic constants are $C_{44}=3.57$ GPa, $C_{55}=11.82$ GPa and $C_{45}=3.74$ GPa. The force constants are $K_1=0.159$ eV/Å^2, $K_2=0.417$ eV/Å^2 and $K_3=0.163$ eV/Å^2. The diagonals are clearly inequivalent and the higher force constant corresponds with the diagonal along the hydrogen bonding network. In the triclinic crystal the nearest neighbour chains are shifted (since $\alpha=105°$) and this coincides with a positive value of K_1. Again, supporting the idea that the chains prefer not to be exactly on top of each other.

It is noteworthy that the average of K_2 and K_3 is 0.29 eV/Å^2, which is 25% higher than K_2 in the bi-directional hydrogen bonding network. This means that the average next-nearest neighbour bonding is stronger in the sheet-like structure. This may indicate that the hydrogen bonds are stronger in this case.

More insight in the role of the nearest and next-nearest neighbour interaction can be obtained by altering the force constants and studying the effect on the internal shear modulus and compressive strength (in fact the upper limit given by the minimal shear stiffness constant).

First the nearest neighbour force constant is altered while fixing the force constants K_2 and K_3. In Fig. 8 the resulting internal shear modulus and compressive strength are shown as function of K_1 for both the triclinic and the monoclinic crystal. It can be clearly seen that the compressive strength at a given K_1 is nearly the same for both crystals. This indicates that nearest neighbour bonding dominates the compressive strength. Also the internal shear modulus depends on K_1 and varies approximately 1 GPa in the plotted range. The difference between the internal shear modulus of the monoclinic crystal and triclinic crystal at a given K_1 is nearly constant (1.6 GPa). Hence, the difference in internal shear modulus (7.7−5.2=2.5 GPa) is caused for 36% (0.9 GPa) by the nearest neighbour interaction, a significant contribution.

The variation of the internal shear modulus and compressive strength upon change of the next-nearest neighbour bonding is plotted in Fig. 9. The solid lines represent the results for the monoclinic structure. The internal shear modulus is strongly dependent on the next-nearest neighbour bonding. Changing $K_2=K_3$ from 0 to 0.5 eV/Å^2 results in a change of internal shear modulus of 12 GPa. Note, that for nearly zero force constants the internal shear modulus vanishes and hence the crystal becomes instable. Actually, in the compressive strength plot it can be seen that the crystal is instable until the force constant K_2 exceeds 0.07 eV/Å^2. This is caused by the negative force constant K_1, which has to be compensated. This critical force constant is more than a factor of three lower than the force constant in the monoclinic crystal (0.232 eV/Å^2) and hence the interchain bonding stabilises the crystal more than sufficiently under shear.

If the force constant K_2 in the monoclinic crystal would take the value of the average of the force constants K_2 and K_3 in the triclinic crystal, a compressive strength of 0.94 GPa would be reached, 1.2 GPa lower than the compressive strength of the triclinic crystal. This difference is caused by the difference in nearest neighbour bonding (K_1).

Also for the triclinic case the internal shear modulus and compressive strength are calculated for varying K_2. In Fig. 9 the results are shown for three fixed values of K_3: The true value 0.163 eV/Å^2, the value of the monoclinic crystal

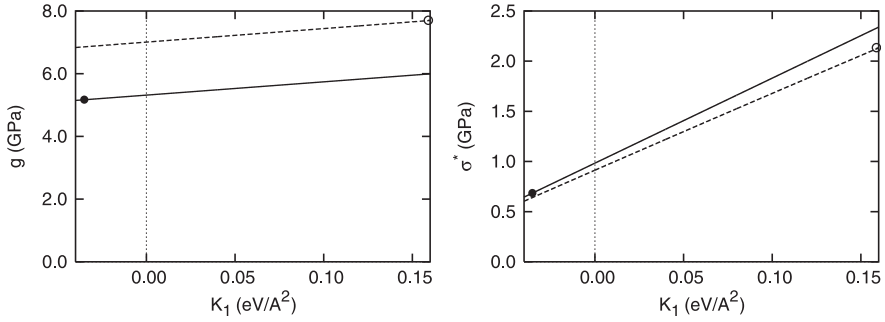

Fig. 8. The internal shear modulus and compressive strength as a function of the nearest neighbour force constant for both the monoclinic crystal (solid line) and the triclinic crystal (dashed line). The full circle represents the monoclinic crystal according to the force constants from the ab initio calculations, the open circle the triclinic crystal.

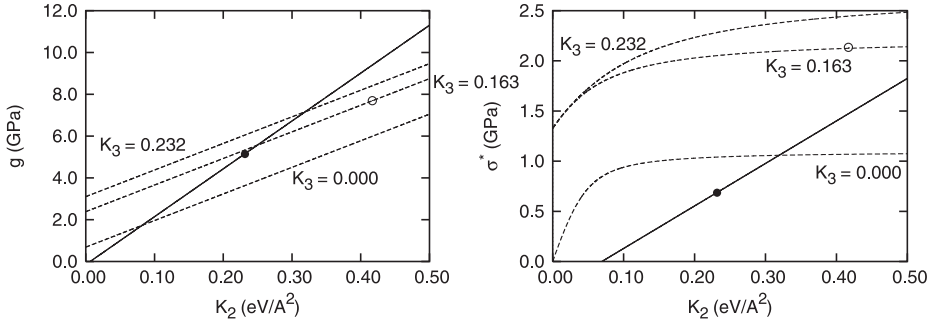

Fig. 9. The internal shear modulus and compressive strength as a function of the next-nearest neighbour force constant K_2. For the monoclinic crystal (solid line) K_3 is equal to K_2. For the triclinic crystal (dashed lines) K_3 is fixed on three values: 0.000, 0.163 and 0.232 eV/Å^2. The full circle represents the monoclinic crystal according to the force constants from the ab initio calculations, the open circle the triclinic crystal.

0.232 eV/Å^2 and for $K_3=0$. The slopes for the three different cases are the same. Hence, the change in the internal shear modulus does not depend on K_3, only the initial value of the internal shear modulus does. The slope of the curves is nearly a factor of two smaller than in the monoclinic crystal, which is a consequence of the fact that for the triclinic crystal only K_2 is varied and K_3 is not. At $K_2=K_3=0.232$ eV/Å^2, the monoclinic values, the internal shear modulus is 6.1 GPa, approximately 1 GPa higher than for the monoclinic crystal, which can be accounted for by the negative nearest neighbour bonding (in the latter).

The compressive strength of the triclinic structure is not linear in K_2. This result stems from the facts that it is equal to the minimal shear stiffness constant and that $C_{45}\neq 0$. The shape of the curve is easily understood for the case that $K_3=0$ [Remember, $K_1\neq 0$]. If K_2 is zero, then the planes formed by the chains 1 and 4 and the chains 5 and 6 can slide past each other without increase of energy. Then the crystal is not stable and the compressive strength is zero. For small K_2 the compressive strength will increase linearly. For large K_2, that is much larger than K_1, the highest stiffness will be found between the planes formed by the chains 1 and 2 and the chains 3 and 6. Increasing K_2 leads to a higher shear stiffness constant for these planes. The lowest shear stiffness constant will be for the other diagonal and it will be K_1 that determines the lowest shear stiffness constant and hence (the upper limit to) the compressive strength. The compressive strength will be constant upon increasing K_2. A cross over between the two regions can be found around $K_2=0.1$ eV/Å^2.

Increasing K_3 to 0.163 eV/Å^2 doubles the limiting compressive strength, since the bonding perpendicular to the plane formed by the chains 2 and 5 is increased. For $K_2=0$ and $K_3>K_1$ the lowest shear stiffness constant is again determined by K_1 analogous to the case that $K_3=0$ and $K_2>K_1$. This explains the fact that for both $K_3=0.163$ eV/Å^2 and $K_3=0.232$ eV/Å^2 the compressive strength is the same for $K_2=0$.

Since K_2 is relatively strong for the triclinic crystal due to the hydrogen bonding, the compressive strength is in the nearly constant region and will hardly depend on the strength of the hydrogen bonding network. It will depend on the other interchain bonding force constants K_1 and K_3. These are sufficiently strong to ensure a compressive strength of 2.1 GPa.

Before going to the conclusions some remarks should be made. This section correlates the calculated shear moduli with interchain bonding. Since bonding is the net interaction, all different interactions may participate in the force constants. This makes it hard to correlate the shear moduli to the hydrogen bonding network. In some cases the correlation can be found; in the triclinic crystal the compressive strength is determined by the force constants K_1 and K_3, which are not in the direction of the hydrogen bonding network. For this reason the network can not participate (directly) in these force constants and hence does not determine (directly) the compressive strength of the triclinic crystal.

The above interpretation should be taken with care, since there may well be an indirect influence of the hydrogen bonding network. For example, in the monoclinic crystal it is the network that stabilises the crystal structure under shear forces. Without the network the chains would shift until the negative nearest neighbour bonding would be positive. In this sense, the network has an indirect influence on all the force constants and hence on the low compressive strength of the monoclinic crystal. Also in the triclinic crystal there may be an indirect influence on the compressive strength, but this is not studied in this section.

In summary, the projection onto the next-nearest neighbour model has shown that not only the hydrogen bonding networks are of importance in the mechanical properties of PIPD. The internal shear modulus and compressive strength are also influenced by those nearest neighbour bindings and next-nearest neighbour bondings that are not due to the network.

7. Discussion and conclusions

In this paper we have presented shear stiffness constants calculated with DFT of two possible crystal structures of

PIPD: The monoclinic crystal with a bi-directional hydrogen bonding network and the triclinic crystal with a sheet-like network. The resulting internal shear modulus (torsion modulus) and upper limit on the compressive strength are compared with the experimental values and are both of the right order of magnitude for both structures. This shows that DFT yields reliable results for these properties.

The calculated shear stiffness constants were analysed with a next-nearest neighbour model. It is shown that the next-nearest neighbour bonding along the direction of the hydrogen bonds is important for the internal shear modulus. It was previously [8] shown that the networks stabilised the crystals and this is confirmed to be particularly true for the stabilisation of the monoclinic crystal under shear. The previously [8] made statement that the high compressive strength can be attributed to the network should be put more carefully.

The monoclinic crystal, which contains the bi-directional hydrogen bonding network, has an internal shear modulus of 5.2 GPa and a (maximal) compressive strength of 0.7 GPa, which can be attributed to the next-nearest neighbour bonding along the network directions. The negative nearest neighbour bonding causes the strength to be lower than in the triclinic crystal. The internal shear modulus is also lower than that in the triclinic crystal. This is partly caused by the negative nearest neighbour bonding, but also by the lower next-nearest neighbour bonding.

The internal shear modulus of the triclinic crystal, containing the sheet-like network, (7.7 GPa) depends on all next-nearest neighbour and nearest neighbour bondings. The compressive strength of 2.1 GPa does not depend (directly) on the next-nearest neighbour bonding in the sheet-like direction, but is mainly determined by the resistance against shear of the bonding between the sheets.

That all interchain interactions should be taken into account is best illustrated by the fact that if only the hydrogen bonding network would be of importance, one would expect the average shear modulus of the two crystals to be the same and the compressive strength of the monoclinic crystal the highest. We have shown that this is not the case: Both the average shear modulus and the compressive strength of the triclinic crystal are significantly higher.

In order to know whether the hydrogen bonding network increases the compressive strength (directly) it is necessary to know the shape of the network: Bi-directional or sheet-like. From the ab initio calculations the following can be concluded on the shape of the network:

1. The total energy calculations show a lower energy for the triclinic crystal containing the sheet-like network. Therefore, the sheet-like network is the most probable based on the total energy calculations. The calculated XRD patterns do not show a clear preference for one of the two ab initio determined structures.
2. For both structures the internal shear modulus of the fibres is calculated. The structure with the bi-directional hydrogen bonding network has a significantly lower modulus than the experimental fibre. The internal shear modulus of the sheet-like structure agrees well with the experimental modulus. Hence, based on the internal shear modulus of the fibre, the sheet-like structure seems to be the most probable.
3. Using the elastic instability theory with the minimal shear modulus as relevant one, the (upper limit on the) compressive strength for the more probable sheet-like structure is predicted to be 2.1 GPa. The experimental strength is only 20% lower and this seems to confirm the elastic instability theory. The bi-directional structure is a factor three weaker (0.7 GPa) than the sheet-like structure.

From the total energy, the internal shear modulus and the compressive strength, we conclude that it is likely that the hydrogen bonding network in the PIPD fibres has the sheet-like shape. As a consequence, it seems plausible that the high compressive strength is not (directly) caused by the strength of the hydrogen bonding network, but by the strong resistance against shear of the bonding between the sheets.

The indirect influence of the hydrogen bonding network is paramount though. This is directly evident when comparing PIPD to a similar polymer crystal lacking any hydrogen-bonded cross-links between the chains, like, e.g. PBO. In one lateral direction one expects a very high resistance against shearing: The PBO chains adjust themselves such that a shearing of π-ring system over π-ring system becomes very unfavourable, like in triclinic PIPD. However, in the perpendicular lateral direction there are no interactions of significant strength between the edges of the ring-systems to counteract a shearing deformation. Thus the compressive strength will be determined by this weak interaction, and not by the resistance against shearing of one π-system over another. Consequently it will be very low.

In triclinic PIPD the situation is entirely different. Within the sheets, easy shearing as in PBO is inhibited by the hydrogen-bond network. Any other shear (that avoids to load the hydrogen bonds) will automatically involve a shear of ring system over ring system. Consequently this rather strong interaction will determine the compressive strength. While in PBO the shear of ring system over ring system is energetically considerably more costly than other shear deformations, in PIPD the presence of the strong hydrogen-bonded network causes it to be the easy shear deformation and thus the limiting factor for the compressive strength.

Somewhat paradoxically the monoclinic PIPD crystal has a much lower compressive strength, although each polymer chain is hydrogen-bonded to no less than four neighbouring chains, compared to only two in the triclinic crystal. However, here more is too much: The ring systems are forced into a relative position that is unfavourable. They want the chains to shift, thus counteracting the hydrogen

bonds. This competition makes that this crystal has a lower compressive strength. This is reflected by the negative nearest neighbour bonding and the apparent weak next-nearest neighbour bonding.

Temperature dependent XRD measurements [4] have shown no splitting of the peaks that correspond to the (110) and $(1\bar{1}0)$ planes. This means that for thermal expansion the two diagonals perpendicular to the chain direction are equivalent. A monoclinic structure would explain this immediately, but the present calculations suggest that the sheet-like structure is more plausible.

A single crystal with sheets running parallel to the (110) planes would show a splitting of the peaks and that is not consistent with the XRD thermal expansion data. For that reason some sheets have to run parallel to the $(1\bar{1}0)$ planes, some parallel to the (110) planes. This requires regions, where crossings have to occur and these may resemble the bi-directional structure. It should be noted that these crossings are then the weaker points of the fibre under compression.

This structure resembles the disorder model as proposed by Klop et al. However, in that model the bi-directional hydrogen bonding network is the basic structure and the sheet-like structure is supposed to be a distortion, while the reverse is proposed on the basis of the present calculations. Moreover, in the crossing regions the monoclinic crystal symmetry will not be fully observed. A crossing region linking one orientation of the triclinic crystal with another orientation is not expected to be crystalline itself. This may offer the freedom to have the relative position of the chains better optimised within the crossing region. Therefore, we expect that the crossing regions will have a higher compressive strength than the perfect monoclinic crystal.

In conclusion, although the hydrogen bonding network is important for the properties of PIPD, it is not possible to neglect the other interchain interactions. The DFT calculations presented here suggest that the PIPD fibres contain a sheet-like hydrogen bonding network and that there is a strong resistance against shearing of the planes. The resulting internal shear modulus and maximal compressive strength are calculated to be 7.7 and 2.1 GPa, respectively, which is in excellent agreement with the experimental values of 7.4 and 1.7 GPa.

Acknowledgements

Stimulating discussions with Dr D. J. Sikkema and Dr M. G. Northolt are gratefully acknowledged. This work is part of the research programme of the Stichting voor Fundamenteel Onderzoek der Materie (FOM) with financial support from the Nederlandse Organisatie voor Wetenschappelijk Onderzoek (NWO).

References

[1] Sikkema DJ. Polymer 1998;39(24):5981–6.
[2] Lammers M, Klop EA, Northolt MG, Sikkema DJ. Polymer 1998; 39(24):5999–6005.
[3] Kozey VV, Jiang H, Mehta VR, Kumar S. J Mater Res 1995;10(4): 1044–61.
[4] Klop EA, Lammers M. Polymer 1998;39(24):5987–98.
[5] Takahashi Y. Macromolecules 2002;35(10):3942–5.
[6] Takahashi Y. Macromolecules 2003;36(23):8652–5.
[7] Tan LS, Arnold FE, Dang TD, Chuah HH, Wei KH. Polymer 1994; 35(14):3091–100.
[8] Hageman JCL, van der Horst JW, de Groot RA. Polymer 1999;40(5): 1313–23.
[9] DeTeresa S, Porter R, Farris RJ. J Mater Sci 1985;20(5):1645–59.
[10] Kresse G, Hafner J. Phys Rev B 1993;47(1):558–61.
[11] Kresse G, Hafner J. Phys Rev B 1994;49(20):14251–69.
[12] Kresse G, Furthmüller J. Comput Mater Sci 1996;6(1):15–50.
[13] Kresse G, Furthmüller J. Phys Rev B 1996;54(16):11169–86.
[14] Perdew JP, Chevary JA, Vosko SH, Jackson KA, Pederson MR, Singh DJ, et al. Phys Rev B 1992;46(11):6671–87.
[15] Kresse G, Hafner J. J Phys: Condens Matter 1994;6(40):8245–57.
[16] Vanderbilt D. Phys Rev B 1990;41(11):7892–5.
[17] Meijer EJ, Sprik M. J Chem Phys 1996;105(19):8684–9.
[18] Nye JF. Physical properties of crystals. Oxford: Clarendon Press; 1960.
[19] Northolt MG. Polymer 1985;26(2):310–6.
[20] Brew B, Hine PJ, Ward IM. Compos Sci Technol 1999;59(7): 1109–16.
[21] Landau LD, Lifshitz EM. Theory of elasticity. 3rd ed. Oxford: Pergamon Press; 1986.
[22] Lacks DJ. J Mater Sci 1996;31(22):5889.
[23] Baltussen JJM, Northolt MG. Polym Bull 1996;36(1):125–31.
[24] Northolt MG, Baltussen JJM, Schaffers-Korff B. Polymer 1995; 36(18):3485–92.